Polymer Journal
https://doi.org/10.1038/s41428-025-01056-2

ORIGINAL ARTICLE

A heuristic study of the Mullins effect in reinforced rubber by using the Weibull distribution

Hiroaki Nobuoka[1] · Osamu Urakawa[1] · Tadashi Inoue[1]

Received: 4 February 2025 / Revised: 31 March 2025 / Accepted: 21 April 2025

Abstract

Stress softening, known as the Mullins effect, has a significant effect on the durability and performance of filler-reinforced rubber, making it a critical issue in designing products for practical applications. While empirical equations are widely used, they fail to capture the intricate and nonlinear behaviors that are characteristic of filler-reinforced rubber. To address this limitation, this study developed a simplified equation to predict the Mullins effect. The model is based on the assumption that the Mullins effect originates from the destruction of particle aggregation structures, and the relationship between the degree of destruction and the stretch ratio is expressed using extreme value statistics. Validation against experimental data revealed that the equation accurately predicts the behavior of rubber reinforced with carbon black (CB) or silica. Additionally, in systems with CB-filled rubber, the equation demonstrated good agreement with the experimental results, even when the CB content was varied. These findings suggest that the proposed model is versatile and effective for predicting the Mullins effect under different conditions, providing a useful tool for understanding and optimizing the performance of filler-reinforced rubber in practical applications.

Introduction

Over the past few decades, rubber has contributed significantly to society as a foundational material. Specifically, it has been widely utilized in various industrial sectors as consumables and consumer goods, such as tires [1], gaskets and sealing materials [2], antivibration rubber products [3], medical rubber products [4], and soles of shoes and sports equipment [5]. The type of rubber used in these products is selected on the basis of their intended applications. For example, natural rubber (NR) or styrene-butadiene rubber (SBR) is employed when high durability and elongation are needed, whereas nitrile-butadiene rubber (NBR) or ethylene propylene diene monomer (EPDM) is used for applications requiring flexibility and adhesion. Similarly, NR or butadiene rubber (BR) is used for impact resistance, and silicone rubber (VMQ) or fluorocarbon rubber (FKM) is chosen for chemical resistance and biocompatibility [6]. Additionally, most rubber products incorporate various fillers to improve their functionality [7]. For example, carbon black (CB) is added to increase strength and impart electrical conductivity [8, 9], silica is used to increase weather resistance and reduce rolling resistance [10, 11], nanoclays contribute to better gas barrier properties [12], titanium dioxide is used to increase heat resistance and provide antibacterial properties [13, 14], and zinc oxide is utilized as a vulcanization accelerator [15].

In general, rubber materials are subjected to repeated loading, necessitating a material design that accounts for such conditions to maintain performance over extended periods. In particular, stress softening in filled rubber materials, known as the Mullins effect, directly impacts the lifespan and performance of rubber, making it a critical issue in product design that considers actual usage environments. The Mullins effect refers to a characteristic phenomenon observed in filled rubber materials, where stress decreases after the first deformation under repeated tension or compression [16]. To elucidate this phenomenon, several hypotheses have been proposed. These include the bond rupture hypothesis [17], which suggests that molecular chains bonded to fillers detach and no longer contribute to elasticity; the molecule slipping hypothesis [18], where molecular chains adhering to fillers slip and cease

✉ Tadashi Inoue
tadashi@chem.sci.osaka-u.ac.jp

[1] Graduate School of Science, Department of Macromolecular Science, The University of Osaka, 1-1 Machikaneyama-cho, Toyonaka, Osaka 560-0043, Japan

Published online: 09 June 2025

contributing to elasticity; the filler rupture hypothesis [19], which attributes the phenomenon to changes in the aggregate structure of fillers; and the disentanglement hypothesis [20], which posits that the stretching process causes disentanglement of molecular chains, leading to reduced elasticity. Despite extensive investigations aimed at understanding the Mullins effect, its physical origins at the molecular scale and the interfacial behavior between the fillers and the matrix remain unclear.

In this context, the prediction of the elastic modulus of filler-reinforced rubber materials often relies on empirical models developed on the basis of experimental data. Models commonly used to predict rubber elasticity include the neo-Hookean model and the Mooney–Rivlin model [21]. These models are widely applied because of their simplicity, as they require relatively few parameters, enabling straightforward analysis of material properties [22]. To account for the Mullins effect, predictive models such as the Ogden–Roxburgh model have been developed [23]. This model is based on the Ogden model but incorporates a damage function to replicate the Mullins effect. However, these predictive models are limited in their ability to address the complex phenomena unique to filler-reinforced rubber materials. To achieve more accurate predictions, models such as the Bergström–Boyce model, which can consider not only elastic behavior but also nonlinear viscoelastic behaviors such as molecular slipping, have been utilized [24]. Nevertheless, this approach is limited by the need for numerous parameters and the complexity of the fitting process, resulting in low versatility and applicability as a general method.

In this study, we address this challenge by developing a simplified predictive model that considers cyclic loading processes. Furthermore, the applicability of the proposed model was evaluated using commonly used materials, specifically CB and silica-filled SBR.

Theory

Overview of reinforcement effects

Before discussing the theoretical aspects, an overview of the experimental data is presented. Here, we focus on the case of uniaxial extension, which is widely used as a method to evaluate the large deformation behavior of rubber. Figure 1 shows the engineering stress–strain curves of rubber with added reinforcing fillers, while the literature was used as a reference for creating Fig. 1 [25]. The nominal strain, ε, is defined as the stretch ratio, λ, expressed by $\varepsilon = \lambda - 1$. Here, Type A represents unfilled rubber, whereas Type B corresponds to rubber reinforced with CB, which exhibits strong interparticle bonding. The addition of reinforcing fillers results in an improved elastic modulus and increased tensile

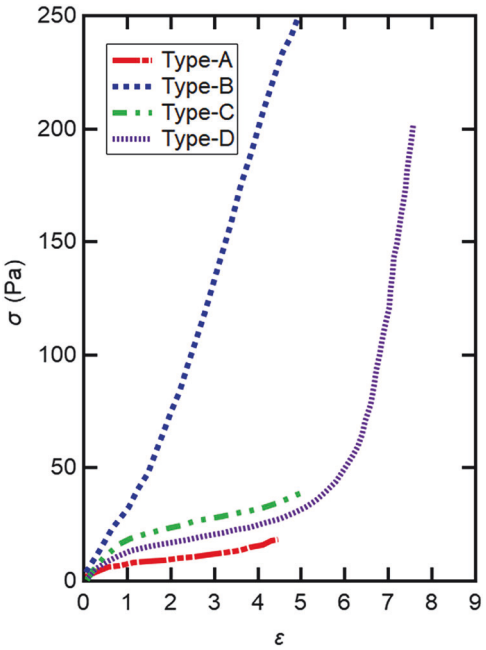

Fig. 1 Stress–strain curves of unfilled rubber (Type A), rubber reinforced with CB (Type B), rubber with large particles exhibiting weak cohesive forces (Type C), and rubber containing partially graphitized CB (Type D). The experimental data were reproduced from Ref. 25

strength. These reinforcement effects are significantly influenced by the properties of CB. Type C represents the case where large particles with weak cohesive forces, such as calcium carbonate, are added. Compared with unfilled rubber, the engineering stress increases by approximately twofold. Type D represents the case where partially graphitized, small CB with low interparticle cohesive forces is added. This analysis highlights the influence of filler properties on the mechanical behavior of rubber, providing a basis for understanding reinforcement mechanisms.

Stretching properties of vulcanized systems

In unfilled rubber, the relationship between stress and strain is described using the neo-Hookean model. Assuming incompressible deformation, the relationship among the engineering stress, σ_e, and the stretch ratio, λ, is expressed by Eq. 1.

$$\sigma_e^M(\lambda) = G\left(\lambda - \frac{1}{\lambda^2}\right) \tag{1}$$

Here, G is the shear modulus, and the superscript M represents the matrix. Furthermore, the Mooney–Rivlin model, shown as Eq. 2, is widely recognized as a universal formula for large deformations.

$$\sigma_e^M(\lambda) = G\left\{\alpha\left(\lambda - \frac{1}{\lambda^2}\right) + (1-\alpha)\left(1 - \frac{1}{\lambda^3}\right)\right\} \tag{2}$$

The value of α is considered to be approximately 0.8 to 0.9. However, in real systems, such as Type A systems, as shown in Fig. 1, the value of α is approximately 0.2. The Mooney–Rivlin model represents the nonlinearity arising from the three-dimensional nature of deformation but does not account for the nonlinearity inherent to the material properties. In such cases, one approach is to introduce the stretch ratio dependency of G and α in Eq. 2. Such approaches are called hyperelastic models, in which the stress–strain relationship is derived from a strain energy density function. In this study, a modified equation, as shown in Eq. 3, was used instead of Eq. 2 to obtain better agreement between the experimental data and equation.

$$\sigma_{\mathrm{e}}^{\mathrm{M}}(\lambda) = G\left(\lambda - \frac{1}{\lambda^2}\right) + G_1\varepsilon_{\mathrm{H}}\exp\left(-\frac{\varepsilon_{\mathrm{H}}}{E}\right) \tag{3}$$

Here, G_1 and E are fitting parameters, and $\varepsilon_{\mathrm{H}} = \ln\lambda$ represents the Hencky strain. Eq. 3 is empirical, and we do not assume the concrete strain energy density function. In this context, Eq. 3 is not a true hyperelastic model.

For reference, the stress–strain curves obtained from each equation are shown in Fig. 2. Here, Finger stands for $\lambda - \frac{1}{\lambda^2}$, and Cauchy stands for $1 - \frac{1}{\lambda^3}$, which appears in Eq. 2. The Mooney–Rivlin model with $\alpha = 0.2$ closely matches the data for the unfilled system (Type A) shown in Fig. 1. Additionally, the second term of Eq. 3 is similar to the Cauchy term at low stretch ratios, but at high stretch ratios, the second term of Eq. 3 yields smaller values than the Cauchy term does. The use of Eq. 3 can be interpreted as a correction to the Mooney–Rivlin model, which tends to overestimate stress in the high stretch ratio region, as shown in Fig. 2. By using Eq. 3, subtle undulations can be reproduced.

Stretching properties of filler-reinforced systems

In filler-reinforced systems, the stretching behavior can be expressed by Eq. 4 on the basis of micromechanics theory, such as the Eshelby/Mori–Tanaka theory [26].

$$\sigma_{\mathrm{e}} = (1 - \phi + a_\sigma\phi)\sigma_{\mathrm{e}}^{\mathrm{M}}(a_\lambda\lambda) \tag{4}$$

Here, a_σ and a_λ represent the stress amplification factor and strain amplification factor, respectively, which are given by Eqs. 5 and 6. The stress, $\sigma_{\mathrm{e}}^{\mathrm{M}}(\lambda)$, represents the stretching characteristics of the matrix rubber and may be described by Eq. 3.

$$a_\sigma = 2.5 \tag{5}$$

$$a_\lambda = \frac{1}{1 - \phi} \tag{6}$$

Thus, if the stretching characteristics of the matrix rubber are given, they can be calculated. However, the

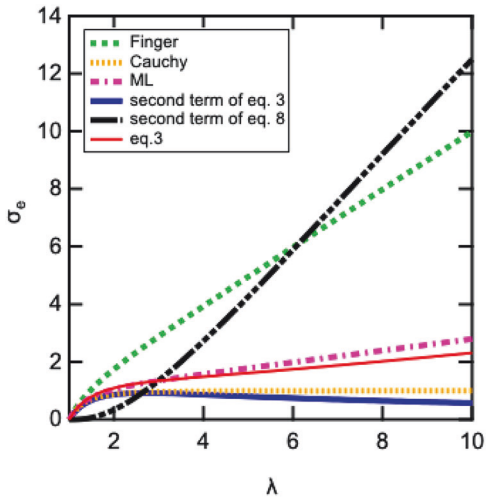

Fig. 2 Stress–strain curves for each equation

Mori–Tanaka theory does not account for interactions between particles [27]. As a result, it tends to underestimate values compared with commonly accepted viscosity equations for particle dispersion systems. To ensure consistency with these viscosity equations for particle-dispersed systems, it is appropriate to consider Eq. 7.

$$a_\sigma = \frac{2.5}{1 - \phi} \tag{7}$$

The effectiveness could be easily checked by numerically comparing the resulting equation (comparing Eq. 4 with Eqs. 6 and 7: $\sigma_{\mathrm{e}}/\sigma_{\mathrm{e}}^{\mathrm{M}} \sim \eta/\eta_0 = 1 + 2.5\phi(1 - \phi)^{-2}$) and the Brinkman or Krieger–Dougherty equation, which are the most reliable viscosity equations for ideal hard-sphere dispersions. However, for the volume fraction, ϕ, it is preferable to use an effective volume fraction, ϕ_{eff}, which accounts for the vitrified layer of rubber on the particle surface. The value of ϕ_{eff} can be determined through DSC measurements [28]. Eq. 3 closely represents the behavior of the matrix rubber, $\sigma_{\mathrm{e}}^{\mathrm{M}}(\lambda)$.

Nonideal stretching properties of aggregating filler systems

In the case of rubber containing cohesive reinforcing particles, the tensile stress may steeply increase in the high-stretch region, leading to strain hardening, as observed in Types B and D in Fig. 1. This strong λ dependence cannot be described by the Finger term $(\lambda - \frac{1}{\lambda^2})$ in Eq. 1, nor can it be represented by the Mooney–Rivlin model. This considerable hardening indicates that strain hardening originates from the nonlinearity of the material itself. The cause of strain hardening is considered to be structural formation due to the association of reinforcing particles. To represent this behavior, it is phenomenologically expressed

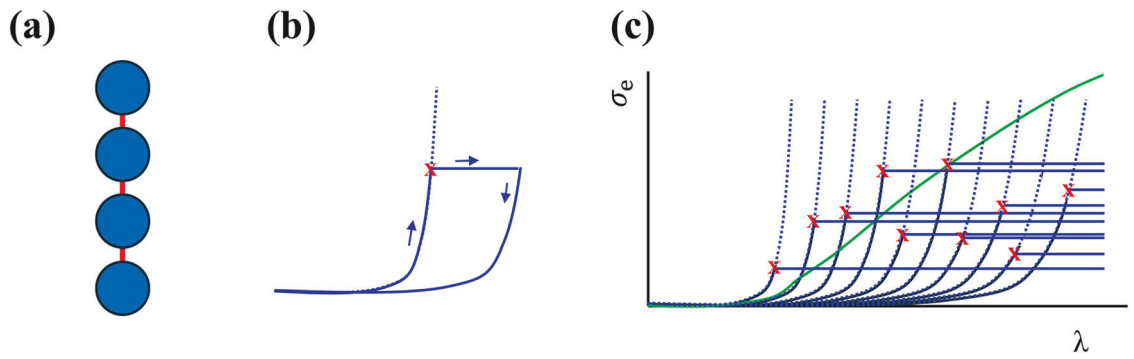

Fig. 3 **a** Section of the network consisting of particles and bridging chains. **b** Stretching of the bridging chains with finite extensibility and their plastic response. The plastic response arises because the anchor points are located in the vitrified (glassy) layer on the surface of the reinforcing particles. **c** Stress–strain curves for individual particles and bridging chains, along with their sum (green line). The sum corresponds to the second term in Eq. 8

by Eq. 8.

$$\sigma_e = (1+B)\sigma_e^M(a_\lambda\lambda) + (C\varepsilon_H)^\beta \tag{8}$$

Here, the first term simplifies the volumetric effect of filler addition, as expressed in Eq. (4), where B is a constant determined by the volume fraction. The second term originates from the aggregated structure of reinforcing particles and expresses the nonlinear increase in stress with changes in strain. The characteristic behavior of the second term is shown in Fig. 2. The stress σ_e from the second term is approximately proportional to λ, but instead of it starting to increase from $\lambda = 1$, it begins to increase after a certain amount of elongation, as shown in Fig. 2. C is a parameter that determines the stretch ratio at which stress begins to increase, whereas β represents the sharpness of the increase, with $\beta = 3$. This delay in stress onset suggests that it originates from the stretching of chains bridging the reinforcing particles. Considering a model in which reinforcing particles are connected by bridging chains, as shown in Fig. 3, the serial model implies the additivity of strain. As a result, the stress does not increase until the longest chain is fully stretched.

A comment may be needed regarding the functional form of the second term in Eq. 8. This form was chosen purely on the basis of a comparison with experimental results. Various functional forms were tested to achieve the best fit with the data. In this study, Eq. 8 accurately describes the experimental results; however, we would not be surprised if different functional forms work well for other systems.

Mullins effect

In stress–strain curves, when rapid strain hardening is observed, the stress–strain curve during unloading does not coincide with that during loading, and hysteresis may be observed (see Fig. 4). This nonlinear effect is known as the Mullins effect. To describe this phenomenon, we assume that the aggregated structure is disrupted during stretching, leading to the loss of $(C\varepsilon_H)^3$ in the second term of Eq. 8. This can be expressed as shown in Eq. 9.

$$\sigma = (1+B)\sigma_e^M(a_\lambda\lambda) + \left[(C\varepsilon_H)^3\right]\Theta(\lambda,\lambda_M) \tag{9}$$

Here, $\Theta(\lambda,\lambda_M)$ represents the fraction of aggregated structures that are disrupted when they are stretched to λ_M. A step function for $\Theta(\lambda,\lambda_{Max})$ can be expressed as shown in Eq. 10.

$$\begin{cases} \Theta(\lambda,\lambda_M) = 0, \lambda < \lambda_M \\ \Theta(\lambda,\lambda_M) = 1, \lambda > \lambda_M \end{cases} \tag{10}$$

When the distribution of the fraction of destruction is considered, $\Theta(\lambda,\lambda_M)$ can be expressed as shown in Eq. 11.

$$\Theta(\lambda,\lambda_M) = \left\{1 - \exp\left[-D\left(\frac{\varepsilon_H}{\varepsilon_H^{Max}}\right)^F\right]\right\} \tag{11}$$

Here, D and F are fitting parameters, and $\varepsilon_H^{Max} = \ln\lambda_{Max}$ represents the maximum strain in each cycle of the test. Eq. 10 represents the Weibull distribution, which is a type of extreme value distribution [29, 30]. It describes the cumulative destruction rate of aggregates under a strain of λ_{Max}. The Weibull distribution is also known as the distribution of the weakest-link model and is utilized to describe the Mullins effect in multiple networks [31–33].

The above discussion is quite a phenomenological one. For a molecular description of the Mullins effect, various models have been proposed [34]. Most of these models assume the elastic energy function $W(J_i)$ of the invariants of strain tensors J_i and consider energy dissipation due to large deformation with various mechanisms. However, the Mullins effect is highly anisotropic, as shown by Urayama

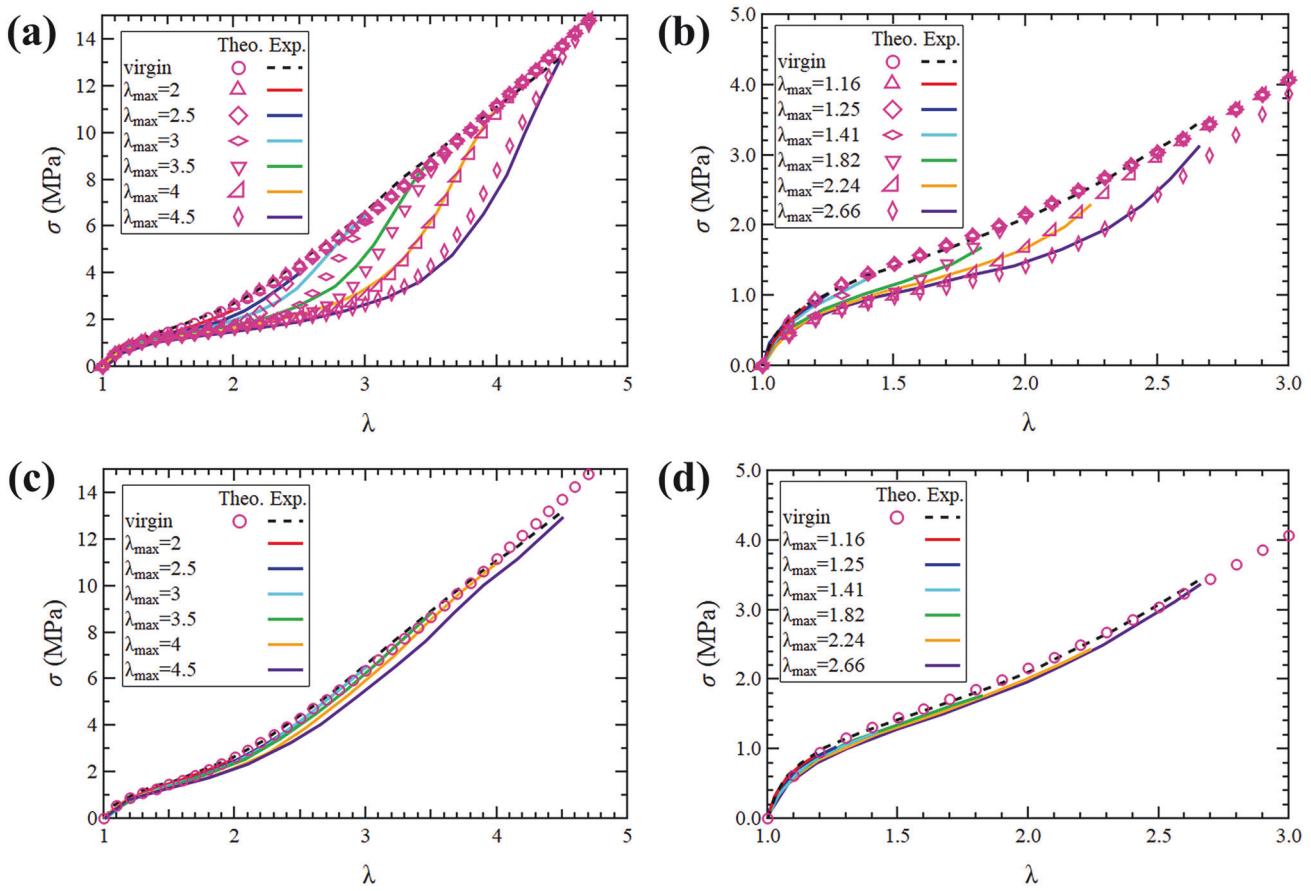

Fig. 4 Comparison of experimental and theoretical values for SBR composites. **a** SBR/CB and **b** SBR/silica: materials exhibiting the Mullins effect (parallel stretching). **c** SBR/CB and **d** SBR/silica: materials not exhibiting the Mullins effect (perpendicular stretching). The experimental data were reproduced from Ref. 35

et al. [35]. Therefore, $W(J_i)$ is not an adequate tool for describing anisotropically damaged samples because it should be used for isotropic materials. Thus, a molecular description of the Mullins effect is still highly challenging.

To capture the molecular origin of the Weibull distribution, let us consider a double network of the rubber network and the glassy network composed of fillers and vitrified rubber. The stress is described as the sum of the contributions of two networks via Eq. 9. A schematic illustration of a strand of the glassy network consisting of particles and bridging chains is shown in Fig. 3a. Upon elongation, the anchor points of the weakest bridging chains detach from the particles, leading to the destruction of the network. The tensile properties of the weakest bridging chain are depicted in Fig. 3b. The second term in Eq. 8 reflects the breaking of the bridging chains in this model. The strong nonlinearity of the second term can be attributed to the stretching of the bridging chains with finite extensibility and the plastic behavior of the vitrified (glassy) layer on the particle surfaces. During elongation, the weakest bridge chains are broken one after another. The function $\Theta(\lambda, \lambda_M)$ corresponds to the survival probability of the bridging chains when they are stretched to λ_M, resulting in the weakest-link model being applicable. We anticipate that a more sophisticated modeling method considering chain statistics would provide a quantitative description, but we need a smart method to address anisotropic materials for further progress.

Comparison with experiments

The applicability of Eq. 9 to different types of fillers was evaluated, and the results are shown in Fig. 4. The experimental data were obtained from the literature and used as a reference to create Fig. 4 [35]. In this study, data were utilized where the Mullins effect was observed in SBR with the addition of 21 vol% CB or silica (equivalent to 50 phr for 100 g of SBR). In this experiment, the samples were first subjected to a predefined amount of uniaxial constrained elongation. After unloading, strip-shaped samples were subsequently cut from the samples parallel and perpendicular to the elongation direction, and uniaxial tensile tests were conducted for each sample. For samples parallel to the

elongation direction, the initial stress during elongation was lower than that of samples without prior uniaxial constrained elongation, indicating the occurrence of the Mullins effect. In contrast, the uniaxial constrained elongation had minimal influence on the samples perpendicular to the elongation direction. Notably, the uniaxial tensile data for unpreloaded samples were consistent with those for Type B samples in Fig. 1, indicating that these data are representative data for the filled rubber samples.

The experimental values agreed well with the predictions (Fig. 4a, b). The parameters used to construct the predictive equations are listed in Table 1. On the other hand, in cases where the Mullins effect does not occur, the behavior can similarly be described using Eq. 9 with $\Theta(\lambda, \lambda_M) = 1$ by setting $\lambda_M = 1$, corresponding to an unpreloaded sample. Here, the maximum strain of the vertical direction in the strain history is $\lambda_M = 1$ in the preloading state rather than $\lambda_M^{-1} < 1$ in the loading state. The results are shown in Fig. 4c, d. Eq. 9 with $\lambda_M = 1$ agreed well with the experimental data (Fig. 4c, d) in the perpendicular direction, which correspond to undamaged samples. These findings demonstrate that the developed predictive equations can effectively estimate the reinforcing effects of CB and silica on rubber, both in the presence and absence of the Mullins effect. The parameter F, referred to as the shape factor in the Weibull distribution, indicates that larger values of F result in sharper distributions. Notably, the silica-based systems presented smaller F values, suggesting a broader strength distribution of the aggregates. The parameter D represents the susceptibility to strain-induced destruction, with smaller D values for silica-based systems implying greater resistance to destruction. Establishing a correlation between structural characteristics and these parameters remains a challenge for future studies.

Furthermore, the applicability of Eq. 9 to cases with different filler contents was evaluated. As in the previous section, the verification was performed using CB-filled SBR. However, due to differences in the amounts of vulcanizing agent and other additives, direct comparison using the fitting parameters from Fig. 4 is not feasible. The experimental data shown in Fig. 5 were obtained from the literature and used as a reference for creating the figure. These include samples with 10 vol% CB added [36], as well as samples with 40 phr (~ 16.8 vol%) CB added to 100 g of SBR [34]. The parameters used to construct the predictive equations are also listed in Table 2. The results confirm that the predicted values agree well with the experimental data, even when the CB content varies.

Our model may be simplified as a 3D jungle gym structure on the basis of the weakest link model and considers complete independence with respect to stress breaks in the chains. In contrast, many existing models attempt to describe the anisotropy of the Mullins effect using a single set of model-specific parameters, although they often fail to do so accurately. Therefore, using separate maximum stretch ratios for each direction, rather than a unified formulation, is crucial for accurately describing the Mullins effect. The Mullins effect can potentially be formulated with a very simple approach that requires fewer parameters. We believe that the simplicity of our model is essential to the effect and an advantage over existing models.

A further comment may be needed concerning the breaking of networks in the previous approaches. A theoretical approach to the Mullins effect was proposed by Ogouari et al. [37]. The key difference between our model and theirs is the treatment of chain breaks. Their model employs the average probability of breakage, whereas ours incorporates extreme value statistics. The significance of

Table 1 Fitting parameters for Eq. 9 in Fig. 4

Filler	Content	G	G_1	E	B	C	D	F
CB	21 vol%	0.65	4	0.23	0.30	1.43	3.0	13
Silica	21 vol%	0.65	4	0.23	0.43	1.00	1.5	6

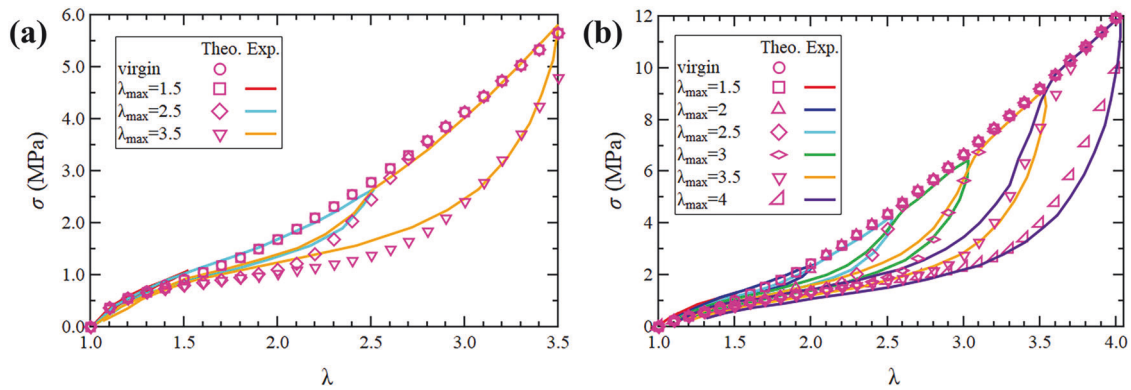

Fig. 5 Comparison of experimental and theoretical values for SBR composites. **a** SBR with 10 vol% CB and **b** SBR with 40 phr (~ 16.8 vol%) CB. The experimental data were reproduced from Ref. 34 and Ref. 36

Table 2 Fitting parameters for Eq. 9 in Fig. 5

Filler	Content	G	G_1	E	B	C	D	F
CB	10 vol%	0.30	2	0.23	0.75	1.25	1.5	10
CB	40 phr	0.30	0.1	0.23	1.50	1.50	1.5	18

extreme value statistics is that they are not governed by values near the mean but by rare events, such as minimum and maximum values. In polymer systems, chain behavior around the mean can often be approximated by a Gaussian distribution; however, under near-extended conditions, deviations from Gaussian behavior become significant, requiring alternative formulations such as the Langevin function. Similarly, in fracture mechanics, the weakest link model is not determined by "the average strength of the links" but rather by the probability distribution of the weakest link itself. The statistical properties of the weakest link differ from those of the mean, making extreme value statistics a crucial tool in modeling fracture behavior. Even in their model, incorporating extreme value statistics for the fracture process may lead to improved results. Additionally, their treatment of reinforcement effects could be refined, as it currently relies on an outdated strain concentration equation.

Finally, the anisotropy of the Mullins effect is discussed. As observed, the destruction of bridging chains is expected to occur under elongation but is less sensitive to compression. This characteristic is often observed in sintered materials, such as ceramics. Under uniaxial constraint and uniaxial elongation deformation, D is large in the elongation direction, and $D \sim 0$ in the constraint direction, which aligns well with the experimental results.

Conclusions

In this study, the Mullins effect was attributed to the destruction of the aggregated structures of reinforcing particles, and the relationship between the degree of destruction and the stretch ratio was expressed via an extreme value distribution. On the basis of this approach, a simplified equation for predicting the Mullins effect was developed. The utility of this equation was validated against experimental data, confirming good agreement for SBR filled with either CB or silica. Furthermore, for CB-filled SBR, the equation was tested in systems with varying CB contents, and similarly, good agreement with the experimental data was observed. These findings verify the effectiveness of the proposed simplified predictive equation for describing the Mullins effect.

Extreme value statistics are commonly used for predicting material failure, and the results of this study strongly suggest that the origin of the Mullins effect lies in the destruction of the aggregated structures of reinforcing particles. The data used for validation were also used to examine the anisotropy of stretching characteristics after uniaxial high elongation, further indicating that the destruction of aggregated structures progresses anisotropically.

Funding Open Access funding provided by The University of Osaka.

Compliance with ethical standards

Conflict of interest The authors declare no competing interests.

Publisher's note Springer Nature remains neutral with regard to jurisdictional claims in published maps and institutional affiliations.

References

1. Thomas BS, Gupta RC. A comprehensive review on the applications of waste tire rubber in cement concrete. Renew Sustain Energy Rev. 2016;54:1323–33.
2. Lin CW, Chien CH, Tan J, Chao YJ, Van Zee JW. Dynamic mechanical characteristics of five elastomeric gasket materials aged in a simulated and an accelerated PEM fuel cell environment. Int J Hydrog Energy. 2011;36:6756–67.
3. Alrashdan A, Alsumait A, Es-Said OS. Material selection of an elastomer capable of absorbing vibrations actuated by a 4D movie theater. J Fail Anal Prev. 2017;17:376–84.
4. Guerra NB, Sant'Ana Pegorin G, Boratto MH, de Barros NR, de Oliveira Graeff CF, Herculano RD. Biomedical applications of natural rubber latex from the rubber tree Hevea brasiliensis. Mater Sci Eng C. 2021;126:112126.
5. Nishi T, Yamaguchi T, Hokkirigawa K. Development of high slip-resistant footwear outsole using rubber surface filled with activated carbon/sodium chloride. Sci Rep. 2022;12:267.
6. Boon ZH, Teo YY, Ang DT-C. Recent development of biodegradable synthetic rubbers and bio-based rubbers using sustainable materials from biological sources. RSC Adv. 2022;12:34028–52.
7. Kohjiya S, Kato A, Ikeda Y. Reinforcement of Rubber. Singapore: Springer Singapore; 2020.
8. Robertson CG, Hardman NJ. Nature of carbon black reinforcement of rubber: perspective on the original polymer nanocomposite. Polym. 2021;13:538.
9. Islam I, Sultana S, Kumer Ray S, Parvin Nur H, Hossain MdT, Md. Ajmotgir W. Electrical and tensile properties of carbon black reinforced polyvinyl chloride conductive composites. J Carbon Res 2018;4:15.

10. Cheraghian G, Wistuba MP. Effect of fumed silica nanoparticles on ultraviolet aging resistance of bitumen. Nanomaterials. 2021;11:1–18.
11. Neethirajan J, Parathodika AR, Hu G-H, Naskar K. Functional rubber composites based on silica-silane reinforcement for green tire application: the state of the art. Funct Compos Mater. 2022;3:7.
12. Cui Y, Kumar S, Rao Kona B, van Houcke D. Gas barrier properties of polymer/clay nanocomposites. RSC Adv. 2015;5:63669–90.
13. Wei K, Feng X, Jiang H, Li C, Hu Y. Improvement of heat resistance in silicone rubber by Fe-doped TiO2 nanoparticles prepared via flame spray pyrolysis. Eur Polym J. 2024;214.
14. Ziental D, Czarczynska-Goslinska B, Mlynarczyk DT, Glowacka-Sobotta A, Stanisz B, Goslinski T, et al. Titanium dioxide nanoparticles: prospects and applications in medicine. Nanomaterials. 2020;10:387.
15. Heideman G, Datta RN, Noordermeer JWM, Van Baarle B. Influence of zinc oxide during different stages of sulfur vulcanization. elucidated by model compound studies. J Appl Polym Sci. 2005;95:1388–404.
16. Diani J, Fayolle B, Gilormini P. A review on the Mullins effect. Eur Polym J. 2009;45:601–12.
17. Bueche F. Molecular basis for the mullins effect. J Appl Polym Sci. 1960;4:107–14.
18. Wan H, Gao K, Li S, Zhang L, Wu X, Wang X, et al. Chemical bond scission and physical slippage in the mullins effect and fatigue behavior of elastomers. Macromolecules. 2019;52:4209–21.
19. Kraus G, Childers CW, Rollmann KW. Stress softening in carbon black-reinforced vulcanizates. Strain rate and temperature effects. J Appl Polym Sci. 1966;10:229–44.
20. Hanson DE, Hawley M, Houlton R, Chitanvis K, Rae P, Orler EB, et al. Stress softening experiments in silica-filled polydimethylsiloxane provide insight into a mechanism for the Mullins effect. Polym. 2005;46:10989–95.
21. Hart-Smith LJ, Crisp JDC. Large elastic deformations of thin rubber membranes. Int J Eng Sci. 1967;5:1–24.
22. Kim B, Lee SB, Lee J, Cho S, Park H, Yeom S, et al. A comparison among neo-hookean model, mooney-rivlin model, and ogden model for chloroprene rubber. Int J Precis Eng Manuf. 2012;13:759–64.
23. Rachid D, Mohand O. On the numerical simulation of damage for the visco-hyperelastic anisotropic behavior of the biomaterials in cyclic loading: relationship of the mullins effect and fibers reinforcement. Procedia Eng. 2015;101:126–34.
24. Bergstrom J. Constitutive modeling of the large strain time-dependent behavior of elastomers. J Mech Phys Solids. 1998;46:931–54.
25. Kraus G. Reinforcement of elastomers by carbon black. Die Angew Makromol Chem. 1977;60:215–48.
26. Douglas Eshelby J. The determination of the elastic field of an ellipsoidal inclusion, and related problems. Proc R Soc Lond A Math Phys Sci. 1957;241:376–96.
27. Mori T, Tanaka K. Average stress in matrix and average elastic energy of materials with misfitting inclusions. Acta Metall. 1973;21:571–4.
28. Inoue T, Narihisa Y, Katashima T, Kawasaki S, Tada T. A rheo-optical study on reinforcement effect of silica particle filled rubber. Macromolecules. 2017;50:8072–82.
29. Weibull W. A statistical distribution function of wide applicability. J Appl Mech. 1951;18:293–7.
30. Zhan L, Qu S, Xiao R. A review on the Mullins effect in tough elastomers and gels. Acta Mech Solid Sin. 2024;37:181–214.
31. Lavoie SR, Millereau P, Creton C, Long R, Tang T. A continuum model for progressive damage in tough multinetwork elastomers. J Mech Phys Solids. 2019;125:523–49.
32. Gumbel EJ. Statistics of Extremes. Columbia University Press; 1958.
33. Boåsen M, Dahlberg CFO, Efsing P, Faleskog J. A weakest link model for multiple mechanism brittle fracture — Model development and application. J Mech Phys Solids. 2021;147:104224.
34. Diaz R, Diani J, Gilormini P. Physical interpretation of the Mullins softening in a carbon-black filled SBR. Polym. 2014;55:4942–7.
35. Mai TT, Taniguchi Y, Tsunoda K, Urayama K. Comparison of mullins effect anisotropy of the elastomers reinforced by carbon-black and silica filler. Nihon Reoroji Gakkaishi. 2023;51:33–9.
36. Liang X. Visualization of nanomechanical properties of polymer composites using atomic force microscopy. Polym J. 2023;55:913–20.
37. Ogouari L, Guo Q, Zaïri F, Mai TT, Urayama K. An anisotropic damage visco-hyperelastic model for multiaxial stress-strain response and energy dissipation in filled rubber. Int J Plast. 2024;182:104111.